Journal of Materials Chemistry C

PAPER

View Article Online
View Journal | View Issue

Cite this: J. Mater. Chem. C, 2014, 2, 3995

Real time observation of mechanically triggered piezoelectric current in individual ZnO nanobelts

A. Asthana,*[a] H. A. Ardakani,[c] Y. K. Yap[b] and R. S. Yassar*[c]

The detection of piezoelectric current in one-dimensional semiconductor materials has been a controversial issue due to the possibility of charge annihilation at nanoscale dimensions. We report here, the mechanically triggered electrical current in uniaxially compressed individual ZnO nanobelts under no applied bias. The measurements were carried out *in situ* by using a transmission electron microscope. In contrast to the bending mode, the magnitude of the electrical current increased with the increase of uniaxial compression, which indicates the load-mode dependency of the detected current. The flow of electrical current through the ZnO nanobelts under applied stress was explained based on the separation of ionic charges along the two ends of the nanobelts due to the applied compressive force. The charge separation is expected to induce an internal electric field inside the nanobelt and facilitate the movement of free charge carriers through the nanobelt. Due to the separation and accumulation of charges, the metal–semiconductor system becomes forward biased when contact is established, leading to the flow of electrons through the Schottky barrier.

Received 7th January 2014
Accepted 3rd March 2014

DOI: 10.1039/c4tc00032c

www.rsc.org/MaterialsC

1. Introduction

The need to develop self-powered nanosystems that can operate wirelessly and independently with a sustainable energy supply has triggered worldwide research on one-dimensional structures with coupled piezoelectricity and conductivity.[1–5] Generally, such nanodevices are fabricated by using individual nanowires/nanotubes/nanobelts having a width of 20–100 nm and a length of a few micrometers. Quasi-one dimensional nanostructures of ZnO, such as nanowires (NWs) and nanobelts (NBs), exhibit both semiconducting and piezoelectric properties.[6] The coupled piezoelectric and semiconducting properties of the NWs and NBs accommodate charge creation, accumulation, and discharge processes. By deflecting or compressing a NB or NW using a conductive atomic force microscope (AFM)/nanoindentator (NI) tip, the energy is first created by the deflection/compressive force and stored by the piezoelectric potential, and later converts into piezoelectric energy. A piezoelectric effect is required to create the electric potential of ionic charges from elastic deformation, and semiconducting properties are necessary to separate and maintain the charges and then release the potential *via* the rectifying behavior of the Schottky barrier at the metal–ZnO interface. Most recently, this approach has been extensively developed to produce usable power output for nanodevices.[3,5]

The recent studies on the piezoresponse of ZnO nanowires show that under bending mode, electrical currents in the range of ~5 nA could be detected from a single nanowire.[2,3,5,7] Subsequently, the current increased continuously with the decrease of bending curvature and the current was stabilized at ~40 nA. The current dropped immediately when the nanowire was bent again. It was suggested that the piezopotential developed across the thickness of the bent nanowires trapped the free electrons and resulted in decrease of electrical conductivity.

There is a controversial issue with respect to the detection of piezoelectric signals (sensor mode) in ZnO nanowires. Earlier work of Hutson[8] shows that the increase in the inherent conductivity of the nanowires can result in reduction of the piezoelectric signal. In this context, Alexe *et al.*[9] predicted that the detection of piezoelectric signals in bent ZnO nanowires may become a very difficult task when the nanowire has high carrier concentrations and low resistance. They based this prediction on the carrier concentration and mobility data obtained for ZnO nanowires by Sirohi *et al.*[10] Alexe *et al.*[9] concluded that in bent nanowires there was a strong driving force (due to the potential across the nanowire diameter) for the free carriers inside the ZnO NW to travel the shortest way (NW diameter) to cancel the displacive charges. However, Wang[11] has shown that the detection of piezoelectric signals will be possible using sensitive measurement systems (total capacity < 10 pF).

Here, we report the mechanically triggered generation of piezoresponse in the uniaxially compressed piezoelectric ZnO nanobelts. In order to correlate the structure–piezoresponse

[a]Department of Material Science & Engineering, Michigan Technological University, Houghton, MI 49931, USA. E-mail: aasthana@mtu.edu

[b]Department of Physics, Michigan Technological University, Houghton, MI 49931, USA

[c]Department of Mechanical Engineering – Engineering Mechanics, Michigan Technological University, Houghton, MI 49931, USA. E-mail: reza@ mtu.edu

properties of a nanobelt, we conducted structural imaging simultaneously with the piezoresponse measurements using a TEM with a conducting probe (capacitance < 3 pF). In the present conductive nanoindentor (NI)/TEM system, the force data are read through a suitable capacitive force sensor with the resolution close to 100 nN and a maximum force of 10 μN can be applied.[12–14] These nanobelts self-ignite electrically once subjected to an externally applied uniaxial compressive load without any external bias. It should be noted that nanobelts with lengths shorter than ~1–2 μm were used in this study to ensure pure compression without bulking and bending of the nanobelts.[15]

2. Experimental procedure

The piezoresponse experiments on ZnO nanobelts were conducted *in situ* with a high resolution TEM using a special NI holder. All the measurements were carried out on a single tilt NI holder using a JEM 4000FX TEM, operating at 200 keV. The detailed description of the NI-TEM holder is reported earlier in our study on the mechanics of ZnO nanowires.[16] The electrochemically etched gold wire with ZnO nanobelts that were attached to the gold tip by conducting silver (Ag) paste was mounted to the piezo-driven movable part of the holder facing the fixed and sharp NI tip. The first step when using the NI-TEM setup is to calibrate the electrical conversion factor (C) of the force sensor. This constant is related to the electrical sensitivity of each sensor and must be set to a value that triggers a 1 : 1 correspondence of the F–d (force–displacement) relationship when the cantilever is tested against the bare substrate of gold. In the present NI system it is 1.01 pF/0.1 μN. In such an arrangement, atomic scale imaging and F–d measurements are carried out concurrently.

The ZnO nanobelts used in our study are grown in a double quartz tube configuration thermal chemical vapor deposition (CVD) system as reported previously but without the use of Au catalyst.[17] The growth was performed in a horizontal furnace consisting of a quartz tube vacuum chamber. A closed end smaller quartz tube (60 cm long and 2 cm in diameter) containing the precursor materials and the substrates was inserted within the vacuum chamber. A mixture of ZnO (0.2 g) and graphite (0.1 g) powder in an alumina boat was used as the precursor material. The boat is placed at the closed end of the smaller quartz tube. A series of low resistance silicon substrates (1–4) was then placed downstream from the mixture in the small quartz tube with a 2 cm spacing in between. Substrates 1 and 4 are 20 cm and 26 cm away from the boat, respectively. Once inserted the closed end of the smaller quartz tube is in the hottest zone of the furnace. The temperature of the furnace was raised to 1100 °C. The substrates were in a temperature zone of ~650 to 450 °C. At ~350 °C, oxygen gas was introduced into the furnace at a 10 sccm flow rate. The temperature was held at 1100 °C for 30 minutes and turned off to allow cooling to 600–700 °C in ~1 hour. The experiment was stopped by switching off the furnace and allowing the system to cool down to room temperature. ZnO NBs were obtained at substrates 1 and 2.[17]

3. *In situ* observation of piezoelectric current

The ZnO nanobelt was examined *in situ* using a high-resolution transmission electron microscope before mechanical straining. The length of the suspension part of the nanobelt was ~2 μm. The width of the nanobelt was measured to be 400 nm (Fig. 1a) and the aspect ratio was estimated to be 8. The TEM analysis revealed that the single crystal structure of the ZnO nanobelt and the growth direction was along [0001] as evidenced by the high-resolution lattice image (Fig. 1b) and the corresponding diffraction pattern (inset of Fig. 1b).

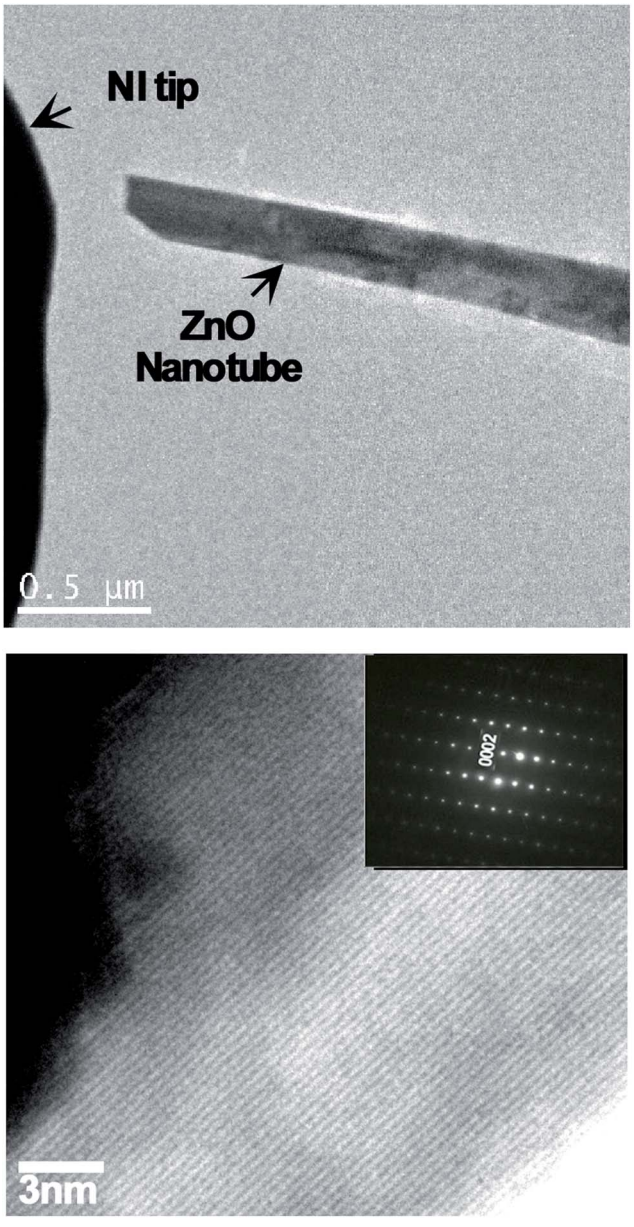

Fig. 1 (a) Bright field TEM image of a ZnO nanobelt attached firmly to the gold wire and approaching the nanoindentor tip; and (b) the high-resolution TEM image and the corresponding diffraction pattern of the ZnO nanobelt.

To ensure the reliability of the recorded data, it is important that the nanobelt be firmly attached to the tip of the gold wire (250 μm diameter) mounted on the piezotube. To ensure this, the nanobelt was attached to the gold tip by silver paste. In order to achieve a good electrical contact between the ZnO nanobelt and the tungsten tip, a field emission process was introduced at the first stage to clean the nanobelt tip and weld the connection. During the field emission, the ZnO nanobelt was kept ~0.5 μm away from the tungsten surface, where 20 V was applied. Under these conditions, the emission current could reach 17 nA. After 1 minute of emission, the high voltage was turned off and the ZnO nanobelt was quickly moved towards the Au tip surface to make a contact. We have repeated this process several times and found that it is very effective for making a reliable electrical contact, possibly due to the high temperature generated at the tip by the emission process as well as desorption of the surface contamination. During the loading and unloading cycles, no slippage at the both ends of the nanobelt was observed.

It is to be noted that to get effective current generation, the metal–nanobelt contact is required to be Schottky in nature. The choice of Au electrodes served as contacts for the current measurements is justified by the Schottky–Mott model, which predicts that metals with high work functions are key candidates for rectifying contacts for n-type semiconductors. Hence, the materials of choice are limited to gold, platinum, and palladium.[18]

Fig. 2a shows the contact of a nanobelt with the NI tip in an uncompressed state. The ZnO nanobelt was moved against the NI tip by the incremental movement of the piezodriven gold tip. As the ZnO nanobelt was strained, a few regions on the nanobelt showed local bright field contrast. The local changes observed, in contrast, may be related to atomic distortion resulting from the stress concentration. Fig. 2b shows the nanobelt under a slightly compressive state (strain, $\varepsilon_1 \sim 5\%$) and the state of the nanobelt with strain, $\varepsilon_2 \sim 10\%$ is shown in Fig. 2c. The nanobelt in the highest compression state ($\varepsilon_3 \sim 25\%$) is shown in Fig. 2d.

The corresponding current variation *versus* time (*I*–*t*) in compressed and uncompressed states in single ZnO nanobelts is shown in Fig. 3a–c. In this measurement, there was no applied bias voltage in the system and the current was continuously recorded while the ZnO nanobelt was slowly compressed against the NI tip. The magnitude of the applied forces is plotted as dashed lines in Fig. 3a–c. As evident in Fig. 3a–c, when the NI tip contacts the nanobelt, the current is almost zero. As the nanobelt is compressed against the NI tip (Region I), there is a continuous increase in the current. When the nanobelt was under 25% compression, the current reached a

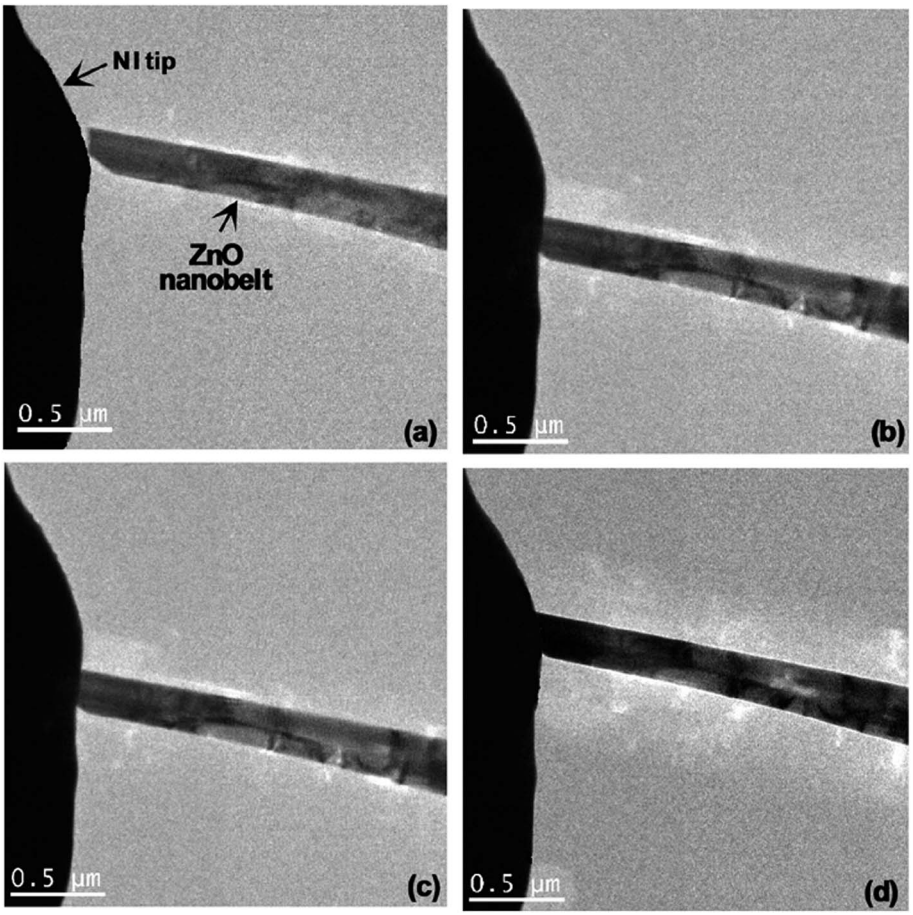

Fig. 2 (a) Bright field TEM image of a ZnO nanobelt in contact with the gold wire and the nanoindentor tip. (b–d) The nanobelt was subjected to a progressive axial force exerted by the incremental movement of the gold wire against the NI tip.

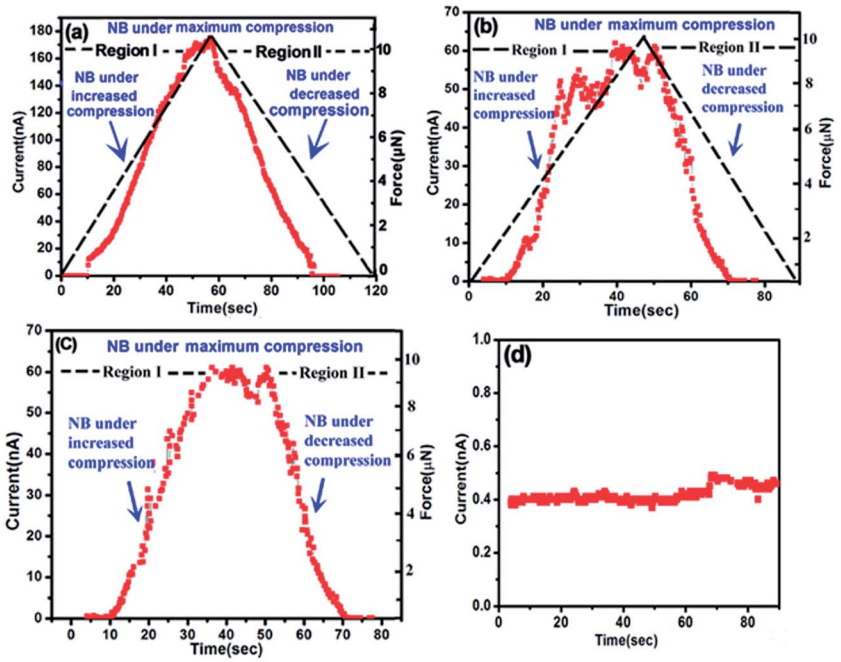

Fig. 3 (a–c) Piezocurrent variation with time during the loading (Region I) and unloading (Region II) of three ZnO nanobelts. All the ZnO nanobelts have similar length but different width dimensions: (a) width of ~400 nm, (b) ~200 nm, and (c) ~200 nm with no electron beam. (d) Current variation with time during the loading and unloading of a Si nanowire.

maximum value of 175.34 nA. During the unloading stage (Region II), the current again slowly drops to almost zero with decrease in the compression along the length of the nanobelt. This detected current is expected to be the result of the piezoelectric potential generated in the nanobelts. We tested several nanobelts in the compression mode and observed a similar behavior of generation of piezocurrent with time. Another such observation for a nanobelt of width ~ 200 nm and length ~ 1 μm is shown in Fig. 3b, where the nanobelt shows an electric current of 67.4 nA under the maximum compression. The behavior of piezoelectric current is consistent with the data reported by Sridhar *et al.*[19] on the current generated during the indentation of PZT-4 and $(Ba_{0.917}Ca_{0.083})TiO_3$ piezoelectric materials. One should note that the charge induced by the mechanical compression is due to the strained contact area and will not be sustained if the contact area is fixed.[19] However, in the case of an advancing contact (*i.e.*, increasing load), the charge buildup increases due to the increase in strained area. Hence, the observed piezoelectric current from the ZnO nanobelt in the present investigation is not transient. If the indentor is conducting and is grounded, a charge opposing that of the specimen would develop. The dynamic change in the charge at the indentor needed to sustain charge neutrality can be measured as a quasi-static current. In a recent study,[20] the piezoelectric coefficient from the ZnO nanowires was measured on the basis of the direct linear piezoelectric response from the substrate integrated ZnO nanowire array devices on galvanized steel.

In order to check the irradiation effect of the electron beam on the piezocurrent, we measured the current versus time of a ZnO nanobelt without the electron beam. We found that there was no change in the value of current with and without the beam as shown in Fig. 3b and c. Fig. 3b shows the *I–t* curve with the beam on and Fig. 3c is the corresponding *I–t* curve with the beam off for the same nanobelt of width ~ 200 nm. However, we found that there is less fluctuation of piezocurrent without the electron beam as shown in Fig. 3c.

A similar experiment on the observation of current by mechanical stress was conducted on a Si nanowire to further clarify whether the detected electrical current is exclusive to ZnO nanobelts. However, the compression of the Si nanowire did not generate any current, in contrast to what we had observed for the case of ZnO nanobelts. The current *versus* time plot of the Si nanowire is shown in Fig. 3d. The Si nanowire is a non-piezoelectric material, hence did not produce any current upon compression. This again indicates that the possibility for the TEM electron beam to be transported through the nanowire and detected by the current measurement setup cannot be the case. The experiment on Si nanowires clarifies that the electrical current observed in ZnO nanobelts under mechanical stress is due to piezoelectricity.

The high-resolution image, before the ZnO nanobelt touches the NI tip, (Fig. 4a) clearly shows that the diffraction contrast at the top of the nanobelt is due to the presence of some dislocation, probably due to mechanical stress when the nanobelt was harvested from the substrate. From the low magnification image, the major part of the nanobelt appears to be free from any defects. The nanobelt in a compressed state (Fig. 4b) shows high bright field diffraction contrast, resulting from atomic distortion due to the high strain field. The high resolution image of the nanobelt at the initial state, *i.e.* before the compression shows highly crystalline and continuous straight

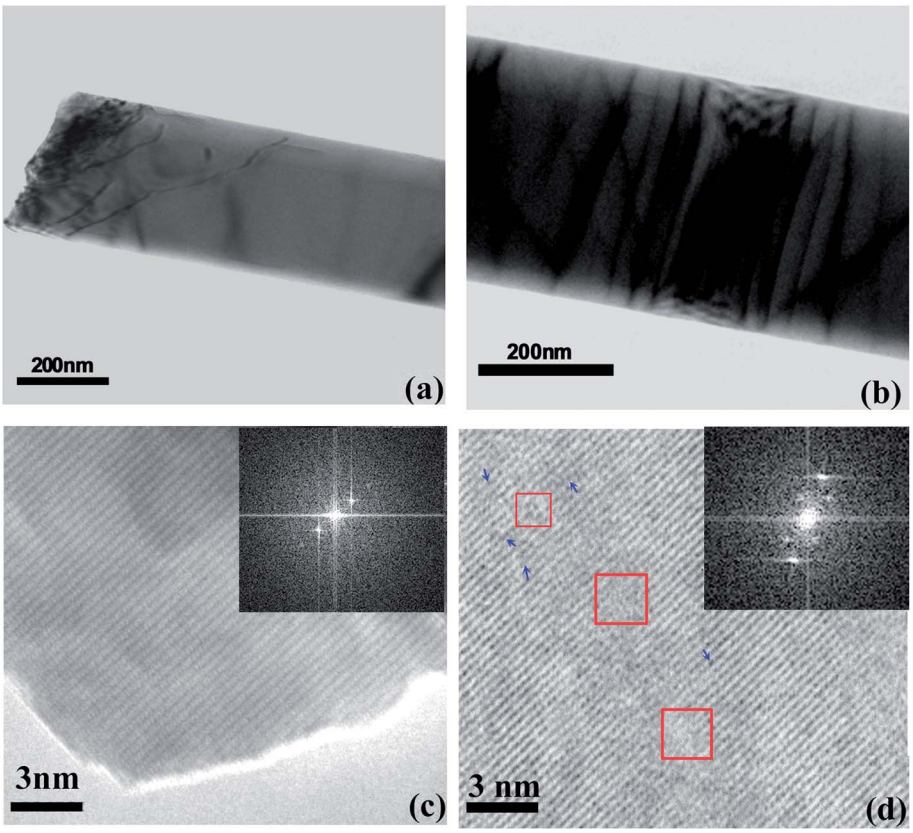

Fig. 4 The high resolution TEM image (a) before the nanobelt contacts the nanoindentor tip, and (b) the same nanobelt under a highly compressive state. Lattice imaging of the nanobelt corresponding to the (c) undeformed state and (d) a highly compressive state is shown.

fringes (Fig. 4c), however after high compression, some regions of the nanobelt show discontinuity in fringes (Fig. 4d) over the few atomic layers (surrounded by red rectangles), which indicates that there is creation of planar defects due to high compression and, also at some point, there is broadening of lattice fringes (some of them are indicated by blue arrows), which might occur due to the creation of point defects. The above observation is also confirmed by the corresponding fast Fourier transform (FFT) patterns. The FFT pattern of the nanobelt in the relaxed state shows sharp and intense diffraction spots (inset of Fig. 4c), however the FFT pattern corresponding to the compressed state shows the diffuse diffraction spots (inset of Fig. 4d), which indicates the presence of planar defects. The formation of defects upon bending of the nanobelt/nanowire has also been reported earlier for ZnO nanowires[21,22] and also for other ceramic and oxide nanowires like SiC, SiO_2, *etc.*,[23,24] These kinds of planar defects and point defects can alter the electronic structure by producing the localized resonant states.[25]

4. Load mode dependency of the electrical potential

Previous studies on the *in situ* electromechanical behavior of ZnO nanowires/nanobelts have shown that the electrical conductivity of the ZnO nanowire/nanobelt decreases upon elastic bending.[7,26–29] However, we observed that the magnitude of electrical current in ZnO nanobelts increases with the increase in applied compressive stress. As observed in Fig. 3a, the current increases to its maximum value (~175.34 nA) under the compression mode with an applied load of ~9.98 μN. It should be noted that our ZnO nanobelts are short (~1–2 μm) as compared to the previously studied ZnO nanowire/nanobelts (~10–20 μm),[30,31] and therefore compression of such nanobelts did not form physical bending on the nanobelt but rather uniaxial compression.

The effect of loading mode on the output piezoelectric signal can be explained by taking into account the effect of deformation modes on the separation of positive and negative ionic charges (Zn^{2+} and O^{2-}).

A piezoelectric material responds to the applied mechanical force by the displacive motion of (+) and (−) charges (Zn^{2+} and O^{2-}) to form a dipole. To better understand the electric potential development in our nanobelts, a series of finite element modeling was performed using COMSOL Multiphysics 4.0A. Zinc oxide nanobelts were modeled as an elastic piezoelectric material with growth along the [0001] direction. A free tetrahedral element was used for meshing the structure. The elastic constant tensor, C, piezoelectric coefficient tensor, e, and dielectric constant tensor, κ, are defined as follows by eqn (1)–(3):

$$C = \begin{bmatrix} 207 & 177.7 & 106.1 & 0 & 0 & 0 \\ 117.7 & 207 & 106.1 & 0 & 0 & 0 \\ 106.1 & 106.1 & 209.5 & 0 & 0 & 0 \\ 0 & 0 & 0 & 44.8 & 0 & 0 \\ 0 & 0 & 0 & 0 & 44.8 & 0 \\ 0 & 0 & 0 & 0 & 0 & 44.6 \end{bmatrix} [\text{G Pa}] \quad (1)$$

$$e = \begin{bmatrix} 0 & 0 & 0 & 0 & -0.45 & 0 \\ 0 & 0 & 0 & -0.45 & 0 & 0 \\ -0.51 & -0.51 & 1.22 & 0 & 0 & 0 \end{bmatrix} [\text{C m}^{-2}] \quad (2)$$

$$\kappa = \begin{bmatrix} 7.77 & 0 & 0 \\ 0 & 7.77 & 0 \\ 0 & 0 & 8.91 \end{bmatrix} \cdot \varepsilon_0 \quad (3)$$

where, $\varepsilon_0 = 8.85 \times 10^{-12}$ F m^{-1} is the vacuum permittivity. In this model, a force was applied at one end while the other end was assumed to be fixed and electrically grounded. Two loading cases were considered: Fig. (5a–c) correspond to the uniaxial compression and Fig. 5(d–f) describe the bending scenario. Fig. (5a–c) show the displacement, d, axial strain, ε, and the corresponding electrical potential, V, of a ZnO nanobelt under the uniaxial compressive loading, F. Under the uniaxial compression, a strain, ε, is developed along the length of the ZnO nanobelt separating the anions (Zn^{2+}) and cations (O^{2-}) in ZnO and polarizing it along the straining direction (shown in Fig. 5c). The polarization can be given by $P = \varepsilon e_{33}$, where e_{33} is the piezoelectric tensor.[32,33] This polarization produces a potential drop of V^+ ($V > 0$) − V^- ($V < 0$) = $|\varepsilon|Le_{33}$ along the length L of the nanobelt.

The modeling results including the displacement, strain, and electrical potential for the bending case are shown in Fig. 5(d–f). There is clear difference in terms of strain and

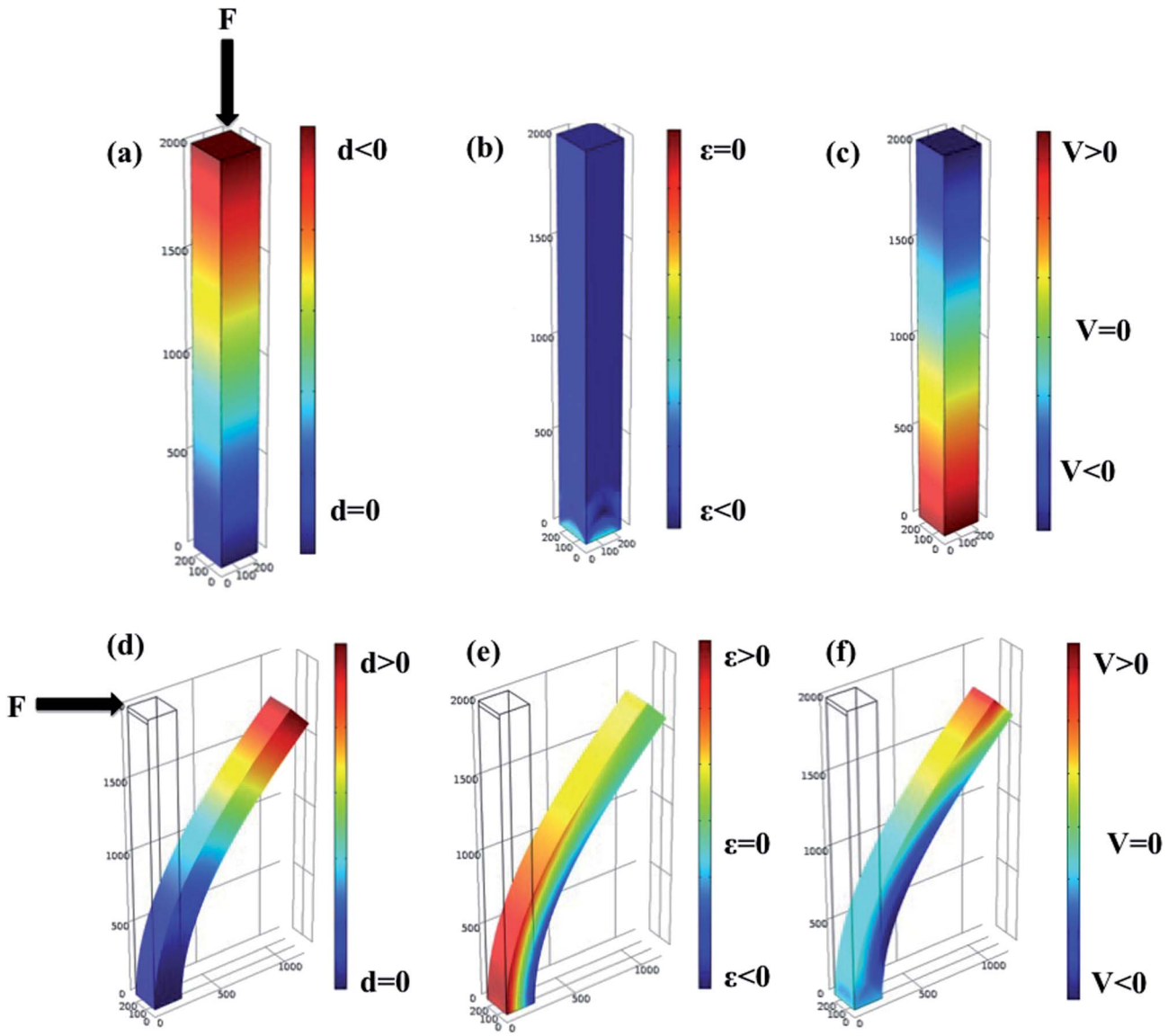

Fig. 5 Finite element simulation of a ZnO NB subjected to (a–c) uniaxial compression and (d–f) cantilever bending: (a and d) displacement contours, (b and e) strain contours, and (c and f) electrical potential contours along the length of the nanobelt are shown.

electrical potential distribution between the two loading scenarios. In the bent NB, formation of tensile and compressive strains results in creation of positive and negative electrical potentials on the outer and inner surfaces, respectively. The modeling results are in agreement with the previous studies on the detection of positive and negative charges on the tension and compressive sides of ZnO nanowires.[34] These ionic charges form an electric field along the width (perpendicular to the axial direction) of the nanobelt, which can trap the free charge carriers and therefore reduce the electrical conductivity. However, under uniaxial compression, the charge separation along the axial direction of the nanobelt can induce an internal electric field inside the nanobelt that assists the movement of charge carriers through the nanobelt resulting in an improvement in electrical conductivity.

The schematic diagram of the model to describe the two mechanisms is shown in Fig. 6. Initially, in the piezoelectric material, (+) and (−) charges form a dipole with slight separation from the center of the dipole (Fig. 6a). When the piezoelectric nanobelt is bent, the charges are separated along the thickness of the nanobelt. The positive charges will be accumulated along the outer arc surface (tension side) and negative charges along the inner arc surface (compressed side). The electric field, E, is generated perpendicular to the length of the nanobelt, and hence perpendicular to the flow of charges. The electrons are trapped in this configuration (Fig. 6b). In the uniaxial compression case, the ionic charges will be separated along the length of the nanowire/nanobelt and form an electric field in the carrier movement direction that gives the driving force for the flow of electrons (Fig. 6c). By the increase of the applied force, more charges will be displaced and hence the magnitude of the electric field increases. Therefore, the magnitude of the detected piezo-current increases by the increase of the applied axial force. The increase in piezoelectric current with time as depicted in Fig. 3 is also due to the increase in the contact area between the NI tip and the nanobelt, when the nanobelt is under increasing compressive stress.

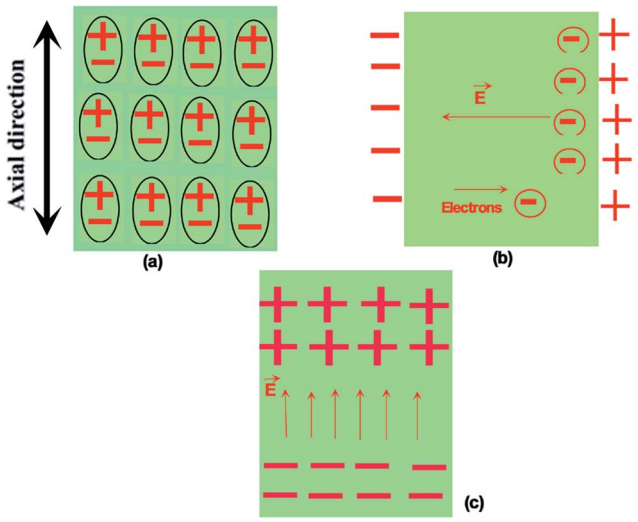

Fig. 6 Schematic diagram of the model depicts (a) the initial state of the piezoelectric material; (b) the state of a bent nanobelt; and (c) the state of a compressed nanobelt.

Our results on ZnO nanobelts are in agreement with those reported by Sridhar *et al.*[19] on PZT and $(Ba_{0.917}\ Ca_{0.083})\ TiO_3$ materials, which shows that when a piezoelectric material is indented towards the poling direction, the induced current increases in magnitude with time, first rapidly and then slowly. This increase is to be expected since the contact area increases with time. The induced current is a result of the electrically polarized contact area.

The piezoresponse observed in nanobelts in our study is explained by linear piezoelectric equations as reported by Sridhar and Giannakopoulos *et al.*[19,35] It is mentioned that mechanical displacement induces a polarization on the piezoelectric specimen at the contact area. By integrating the electric charge distribution under the indentor, an expression for the mechanically induced total charge, Q, is found as

$$Q = \frac{16}{3} M_1 \frac{a^3}{D} + 2\pi a \left[\varnothing_0 M_2 - M_1 \left(h - \frac{2a^2}{D} \right) \right] \quad (4)$$

The charge distribution (eqn (4)) under the indentor is due to the strained contact area and will not be sustained if the contact area is fixed. However, in the case of an advancing contact *i.e.*, spherical indentation with increasing load, the charge buildup increases due to the increase in strained area. If the indentor is conducting and is grounded, a charge opposing that of the specimen would develop. The dynamic change in the charge at the indentor needed to sustain charge neutrality can be measured as a quasi-static current. The constants M_1 and M_2 depend in a complicated way on the five elastic (c_{ij}^E), two dielectric (ε_{ij}^T), and three piezoelectric (e_{ij}) constants that characterize the material.[35,20] The parameters, ϕ is an electric potential, a is the contact radius and h is the displacement corresponding to the rigid sphere of diameter D.

It is to be noted that the piezoelectric current would not increase infinitely with increasing compressive stress. The increase of compressive stress beyond some threshold value will induce mechanical instability in the nanowires, which eventually may result in fracture. Therefore, the magnitude of stress was kept in a linear regime.

5. Contact resistance and the detection of piezoelectric current

The Schottky contact between the metal and the semiconductor (M–S) ZnO nanobelt is one of the key factors that can affect the detection of the piezo-current signal. Schottky barriers can form at metal–semiconductor (M–S) interfaces. According to the configuration of both metallic contacts and the ZnO NB, it can be considered that the piezoelectric current produced by the compression of the ZnO nanobelt flows through an M–S–M (Metal–Semiconductor–Metal) circuit. One of the contacts is Schottky and is formed between the conductive NI tip (Au coated) and the ZnO nanobelt (n type semiconductor) and the other is Ohmic formed between the Ag paste and the ZnO

nanobelt. The nonlinear current–voltage (I–V) behavior is predicted if both the contacts are Schottky-type, however, we have observed a nonlinear I–V behavior from the ZnO nanobelt, even if one contact is Schottky and the other is Ohmic. The reason for this barrier can be the interface layer or the surface layer of ZnO at the contact.

As predicted by the simulation, when the ZnO nanobelt was subjected to uniaxial compression (Fig. 5a–c), the ionic charges will be separated along the axial length of the nanobelt and form a polarized electric field in the direction of carrier movements in the M–S–M circuit. The schematic representation of the process with the corresponding band structure is shown in Fig. 7(a and b). Fig. 7(a) shows the uncompressed ZnO nanobelt with one end grounded and the other end to be pushed against a conducting NI tip. The corresponding band structure diagram illustrates the formation of the Schottky barrier $\phi_{\text{Au-NB}}$ at the metal (Au tip)–n type semiconductor (ZnO nanobelt) contact, and an Ohmic contact at the metal Ag–n type semiconductor interface. Fig. 7(b) depicts the ZnO nanobelt in a compressed state. In a compressed state there will be separation of charges and the Schottky barrier *i.e.* $\phi_{\text{Au-NB}}$ can become forward biased when the (−) charges accumulate at the STM tip and the ZnO nanobelt interface. The electrons will flow easily through the Ohmic contact formed between the (Ag)–n type semiconductor completing the M–S–M circuit. A similar observation of flow of current through a forward biased Schottky diode has been reported by Wang *et al.*[2] for the bending of the ZnO nanowire by *in situ* AFM experiments.

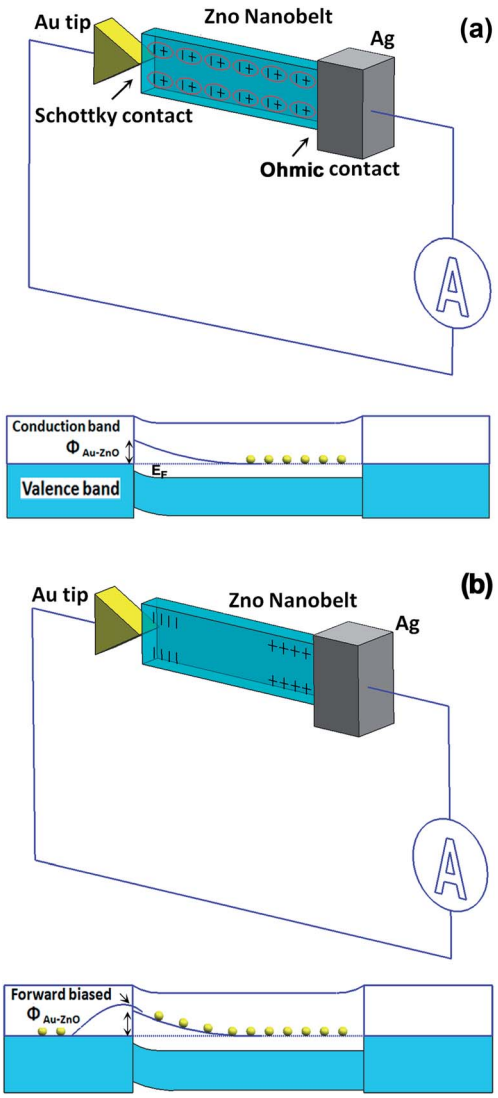

Fig. 7 Schematic diagram of an (a) uncompressed ZnO nanobelt with one end grounded and the other end to be pushed against a conducting NI tip. The band structure diagram shows the formation of the Schottky barrier at the metal (Au tip)–n type semiconductor (ZnO nanobelt) and an Ohmic contact at the metal Ag–ZnO nanobelt; and (b) a ZnO nanobelt in the compressed state. The band diagram illustrates that one of the Schottky barriers is forward biased and the electrons flow through the barrier.

The Schottky barrier height can also be modulated under mechanical straining.[36–40] This relationship can be defined as in eqn (5) below

$$\ln[I(\varepsilon)/I(0)] = -\Delta\phi/kT \quad (5)$$

where $I(\varepsilon)$ and $I(0)$ are the currents measured through the ZnO nanowire at a fixed bias with and without being strained, respectively. This indicates that the change of Schottky barrier height, $\Delta\phi$, has an approximately linear relationship with strain. From the above argument, we can conclude that the Schottky barrier height can be reduced due to the straining of the ZnO nanowire and this further assists the flow of electrons through the M–S–M circuit.

In many reported studies on piezoelectric behavior of ZnO nanostructures, PVP and PZT materials,[2,3,5,7,26–29,41,42] the piezoelectric charges manifest themselves as transients of current. This is true when the piezoelectric materials are introduced with periodical on–off strains as reported by Chang *et al.*,[41] Chen *et al.*[42] and Zhang *et al.*[26–29] Going through the above mentioned studies, we have found that the strains applied on the ZnO nanowires, PVP and PZT materials are periodic and thus lead to transient flow of piezocurrent in response to the on–off strains. This is clearly different from our case. In our experimental work, we observed an increasing piezoelectric current when the ZnO nanobelt was under an increasing strain at a constant rate. We then observed a decreasing piezoelectric current when we release the strain at a constant rate. Our detected current follows the magnitude of the applied strain since forces are always applied and piezo-potential is always present as a result of charge separation in a piezoelectric material.

It is to be noted that we have taken enough care to minimize the irradiation effects of the electron beam on the generation of piezocurrent in our present study in the ZnO nanobelt. We made efforts to eliminate the effect of the electron beam by conducting the structural characterization at a low beam current of 2.91 nA and study the piezoelectric current at even lower beam current of 0.72 nA. The low beam currents of 0.72 nA and 2.91 nA were obtained by adjusting the possible combination of the condenser aperture and spot size. The electron beam was spread to avoid any convergence of the beam on the sample. In addition, we shut off the electron beam while

recording *I–V* data. Thus, the related contamination and electron beam induced effect on piezocurrent is decently minimized. Similar concerns about the effect of the electron beam have also been reported by Bai *et al.*[43] and Han *et al.*[44] Han *et al.* carried out a similar *in situ* experiment at 200 kV with a low beam current and found through simple calculation[45] that the local temperature is no more than a few degrees above room temperature. We did not observe any appreciable change in *I–V* data after repeating the cycles a few times and it proves that the nanobelt is not affected by the electron beam during the time it is under the electron beam for manipulation and *I–V* acquisition. In some of our previous studies,[15] the low current beam radiation did not induce any detectable change in the conductivity of the nanobelts indicating that the effect of electron beam can be ignored in the analysis of the data presented in this work.

6. Conclusion

In conclusion, under no external bias, piezoelectric current could be generated in a single ZnO nanobelt by mechanically compressing it using a conductive force probing system. The mechanically triggered electrical response increases with the increase in the uniaxial compressive deformation. The mechanism behind this observation of piezoresponse under compressive stress is due to the separation of ionic charges (Zn^{2+} and O^{2-}) along the stress axis. This charge separation leads to the generation of an electric field inside the nanobelt and assists the carrier charges to move through the nanobelt without any external bias. Due to the separation and accumulation of charges at the metal–ZnO nanobelt end, one of the metal–semiconductor contacts becomes forward biased, leading to the flow of electrons through the barrier. The increase of applied compressive force will further separate the charges and increase the polarization potential. This will increase the electric field and hence the driving force for the flow of free charge carriers. The increase in piezoelectric current with time can also be mediated with the increase in the contact area between the nanoindentor tip and the nanobelt, when the nanobelt is under increasing compressive stress.

Acknowledgements

The authors would like to acknowledge the funding support through the NSF-DMR grant no. 0820884 and NSF-CMMI grant no. 0926819.

References

1 U. Ozgur, Y. I. Alivov, C. Liu, A. Teke, M. A. Reshchikov, S. Dogan, V. Avrutin, S. J. Cho and H. Morkoc, *J. Appl. Phys.*, 2005, **98**, 041301.
2 Z. L. Wang, *Adv. Funct. Mater.*, 2008, **18**, 3553.
3 J. Zhou, P. Fei, Y. Gao, Y. Gu, J. Liu, G. Bao and Z. L. Wang, *Nano Lett.*, 2008, **8**, 2725.
4 S. Xu, Y. Qin, C. Xu, Y. Wei, R. Yang and Z. L. Wang, *Nat. Nanotechnol.*, 2010, **5**, 366.
5 X. Wang, J. Zhou, J. Song, J. Liu, N. Xu and Z. L. Wang, *Nano Lett.*, 2006, **6**, 2768.
6 Z. L. Wang, *J. Phys.: Condens. Matter*, 2004, **4**, 423.
7 S. Yang, L. Wang, X. Tian, Z. Xu, W. Wang, X. Bai and E. Wang, *Adv. Mater.*, 2012, **24**, 4676.
8 A. R. Hutson, *Phys. Rev. Lett.*, 1960, **4**, 505.
9 M. Alexe, S. Senz, M. A. Schubert, D. Hesse and U. Gosele, *Adv. Mater.*, 2008, **20**, 4021.
10 J. Sirohi and I. Chopra, *J. Intell. Mater. Syst. Struct.*, 2000, **11**, 246.
11 Z. L. Wang, *Adv. Mater.*, 2009, **27**, 1311.
12 M. A. Wall and U. Dahmen, *Microsc. Res. Tech.*, 1998, **42**, 248.
13 E. A. Stach, T. Freeman, A. M. Minor, D. K. Owen, J. Cumings, M. A. Wall, T. Chraska, R. Hull, J. W. Morris, A. Zettl Jr and U. Dahmen, *Microsc. Microanal.*, 2001, **7**, 507.
14 A. M. Minor, J. W. Morris and E. A. Stach, *Appl. Phys. Lett.*, 2001, **79**, 1625.
15 A. Asthana, K. Momeni, A. Prasad, Y. K. Yap and R. S. Yassar, *Appl. Phys. Lett.*, 2009, **25**, 172106.
16 A. Asthana, K. Momeni, A. Prasad, Y. K. Yap and R. S. Yassar, *Nanotechnology*, 2011, **22**, 265712.
17 S. L. Mensah, V. K. Kayastha and Y. K. Yap, *J. Phys. Chem. C*, 2007, **111**, 16092.
18 B. J. Coppa, C. C. Fulton, S. M. Kiesel, R. F. Davis, C. Pandarinath, J. E. Burnette, R. J. Nemanich and D. J. Smith, *J. Appl. Phys.*, 2005, **97**, 103517.
19 S. Sridhar, A. E. Giannakopoulos, S. Suresh and U. Ramamurty, *J. Appl. Phys.*, 1999, **85**, 380.
20 J. M. Velazquez, S. Baskaran, A. V. Gaikwad, T. Ngo-Duc, X. He, M. M. Oye, M. Meyyappan, T. K. Rout, J. Y. Fu and S. Banerjee, *Appl. Mater. Interfaces*, 2013, **5**, 10650–10657.
21 H. Xiaobing, J. Guangyin, Z. Xinzheng, M. Renmin, S. Xuefeng, X. Jun, L. Zhimin, W. Ning and Y. Dapeng, *Nano Res.*, 2009, **2**, 553.
22 Y. Ding and Z. L. Wang, *J. Phys. Chem. B*, 2004, **108**, 12280.
23 X. D. Han, Y. F. Zhang, K. Zheng, Z. Zhang, Y. J. Hao, X. Y. Guo, J. Yuan and Z. L. Wang, *Nano Lett.*, 2007, **7**, 452.
24 K. Zheng, X. Han, L. Wang, Y. Zhang, Y. Yue, Y. Qin, X. Zhang and Z. Zhang, *Nano Lett.*, 2009, **9**, 2471.
25 W. A. de Heer, J. M. Bonard, K. Fauth, A. Chatelain, L. Forro and D. Ugarte, *Adv. Mater.*, 1997, **9**, 87.
26 K. H. Liu, P. Gao, Z. Xu, X. D. Bai and E. G. Wang, *Appl. Phys. Lett.*, 2008, **92**, 213105.
27 Y. Liu, Z. Y. Zhang, Y. F. Hu, C. H. Jin and L.-M. Peng, *J. Nanosci. Nanotechnol.*, 2007, **8**, 1.
28 X. Lin, X. B. He, T. Z. Yang, W. Gao, D. X. Shi, H.-J. Gao, D. D. D. Ma, S. T. Lee, F. Liu and X. C. Xie, *Appl. Phys. Lett.*, 2006, **89**, 043103.
29 P. M. F. J. Costa, D. Goldberg, G. Shen, M. Mitome and Y. Bando, *J. Mater. Sci.*, 2008, **43**, 1460.
30 M. Huang, P. Rugheimer, M. G. Lagally and F. Liu, *Phys. Rev. B: Condens. Matter Mater. Phys.*, 2005, **72**, 085450.
31 Q. H. Li, Q. Wan, Y. X. Liang and T. H. Wang, *Appl. Phys. Lett.*, 2004, **84**, 4556.
32 M. H. Zhao, Z. L. Wang and S. X. Mao, *Nano Lett.*, 2004, **4**, 587.

33 J. F. Nye, *Physical Properties of Crystal*, Oxford University Press, London, 1957.
34 J. Zhou, P. Fei, Y. Gao, Y. Gu, J. Liu, G. Bao and Z. L. Wang, *Nano Lett.*, 2008, **8**, 2725.
35 A. E. Giannakopoulos and S. Suresh, *Acta Mater.*, 1999, **47**, 2153.
36 J. Appenzeller, M. Radosavljevic, J. Knoch and P. Avouris, *Phys. Rev. Lett.*, 2004, **92**, 048301.
37 J. Zhou, Y. Gu, P. Fei, W. Mai, Y. Gao, R. Yang, G. Bao and Z. L. Wang, *Nano Lett.*, 2008, **8**, 3035.
38 Y. Liu, Z. Kauser, P. P. Ruden, Z. Hassan, Y. C. Lee, S. S. Ng and F. K. Yam, *Appl. Phys. Lett.*, 2006, **88**, 022109.
39 W. Shan, M. F. Li, P. Y. Yu, W. L. Hansen and W. Walukiewicz, *Appl. Phys. Lett.*, 1988, **53**, 974.
40 K. W. Chung, Z. Wang, J. C. Costa, F. Wiliamson, P. P. Ruden and M. I. Nathan, *Appl. Phys. Lett.*, 1991, **59**, 1191.
41 C. Chang, V. H. Tran, J. Wang, Y.-K. Fuh and L. Lin, *Nano Lett.*, 2010, **10**, 726.
42 X. Chen, S. Xu, N. Yao and Y. Shi, *Nano Lett.*, 2010, **10**, 2133.
43 X. D. Bai, D. Goldberg, Y. Bando, C. Y. Zhi, C. C. Tang, M. Mitome and K. Kurashima, *Nano Lett.*, 2007, **7**, 632.
44 X. D. Han, Y. F. Zhang, K. Zheng, X. N. Zhang, Z. Zhang, Y. J. Hao, X. Y. Guo, J. Yuan and Z. L. Wang, *Nano Lett.*, 2007, **7**, 4529.
45 I. Jencic, M. W. Bench and I. M. Robertson, *J. Appl. Phys.*, 1995, **78**, 974.